Supplementary Information for

Open-state structure of veratridine-activated human $Na_V1.7$ reveals the molecular choreography of fast inactivation

Xiao Fan[1,4,5], Jiaofeng Chen[2,4], Lingfeng Xue[3,4], Huan Wang[2], Tong Wu[2], Xiaoshuang Huang[1], Fangzhou Lu[1], Xueqin Jin[2], Chen Song[3,5], Jian Huang[1,5], and Nieng Yan[1,2,5]

[1]Institute of Bio-Architecture and Bio-Interactions (IBABI), Shenzhen Medical Academy of Research and Translation, Guangming District, Shenzhen 518107, Guangdong, China

[2]Beijing Frontier Research Center for Biological Structures, State Key Laboratory of Membrane Biology, Tsinghua-Peking Joint Center for Life Sciences, School of Life Sciences, Tsinghua University, Beijing 100084, China

[3]Center for Quantitative Biology, Academy for Advanced Interdisciplinary Studies, Peking University, Beijing 100871, China

[4]These authors contribute equally.

[5]To whom correspondence should be addressed: Nieng Yan (nyan@tsinghua.edu.cn), Jian Huang (huangjian@smart.org.cn), Chen Song (c.song@pku.edu.cn), and Xiao Fan (xfan@smart.org.cn).

The PDF file includes:

Supplementary Figures S1 to S7
Supplementary Tables S1 to S5
Supplementary Videos S1 to S2

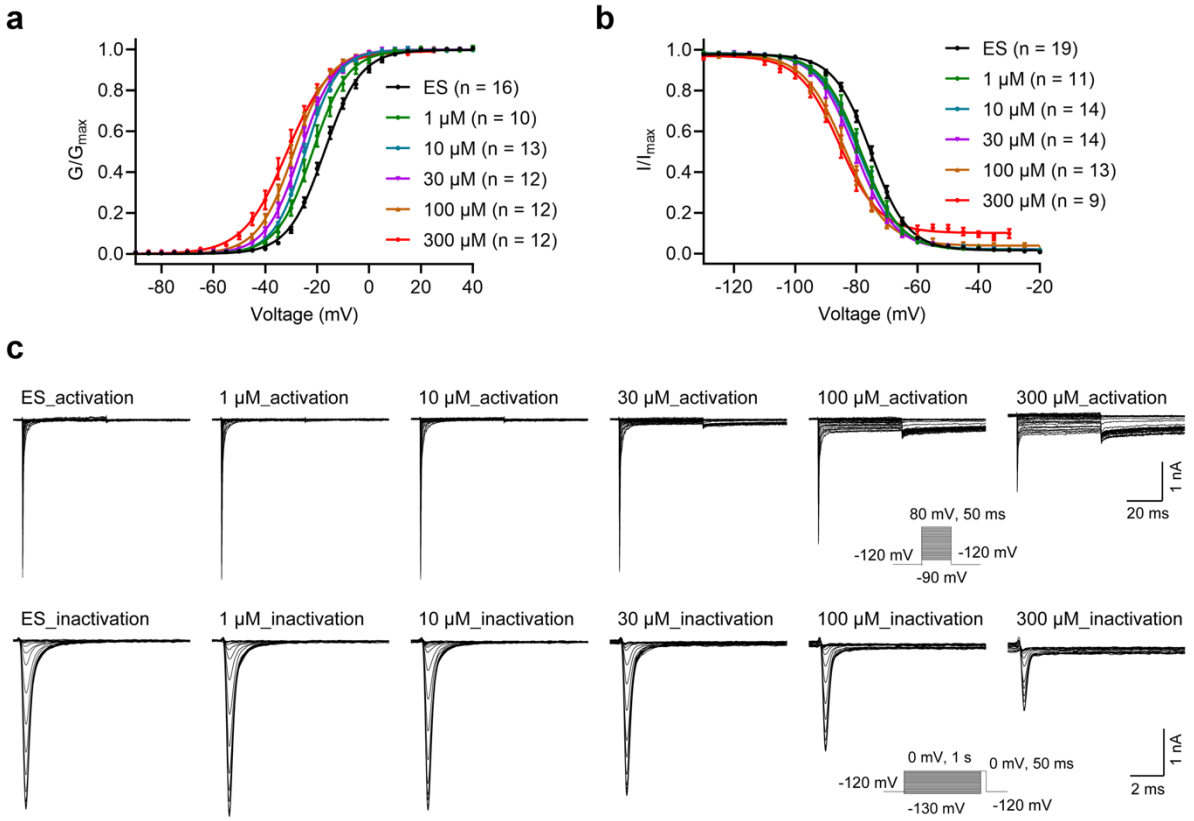

Supplementary Figure S1 | Functional characterization of veratridine modulation of human $Na_v1.7$. (**a**) Voltage-dependent activation curves and (**b**) steady-state inactivation curves of $Na_v1.7$ recorded at varying concentrations of veratridine. (**c**) Representative current traces showing voltage-dependent activation (*top*) and steady-state inactivation (*bottom*) of $Na_v1.7$ in the presence of veratridine at the indicated concentrations. Insets show the corresponding recording protocols.

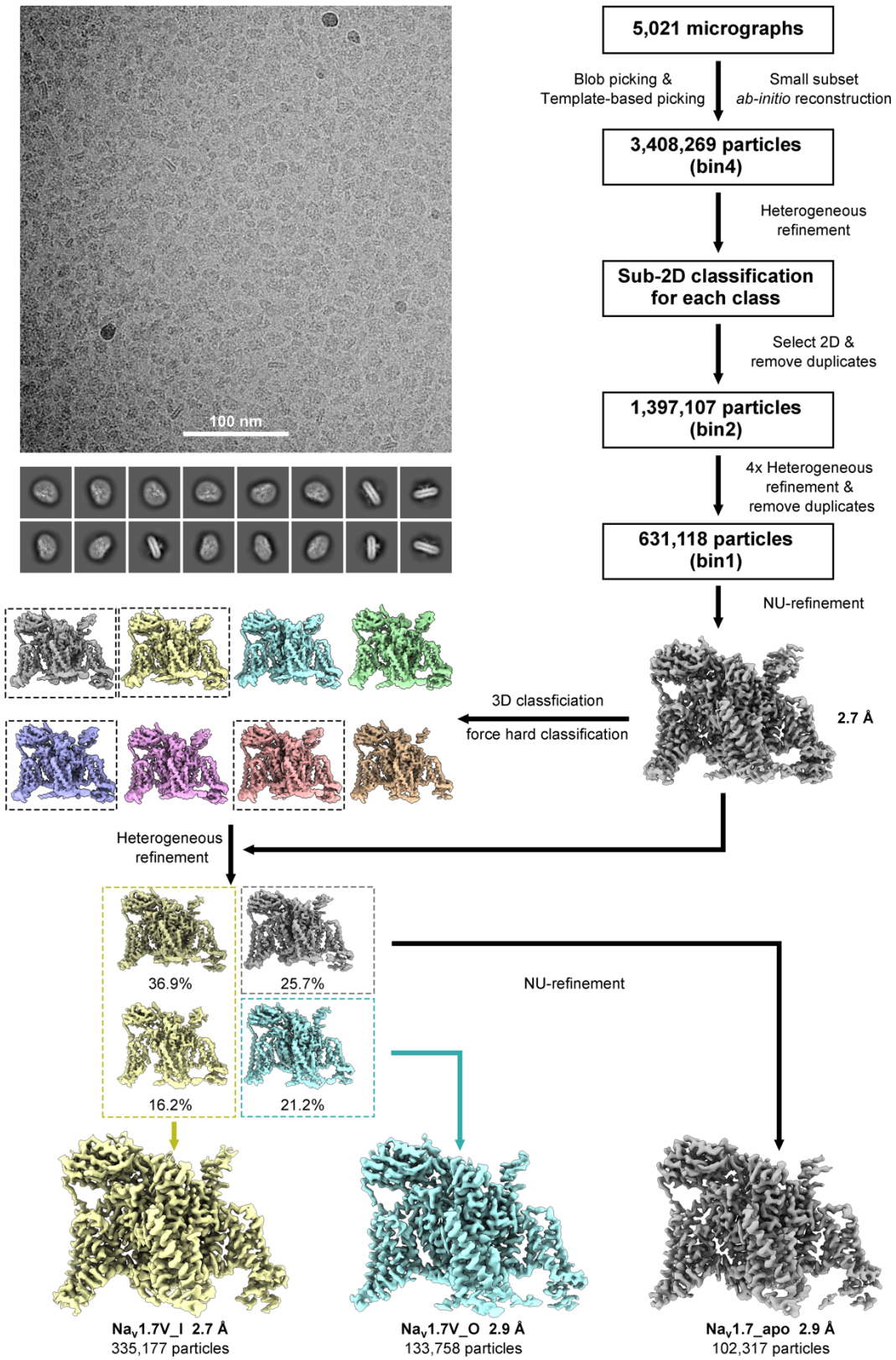

Supplementary Figure S2 | Cryo-EM data processing workflow. A representative raw micrograph and corresponding 2D class averages are shown. Details are provided in *Materials and Methods*.

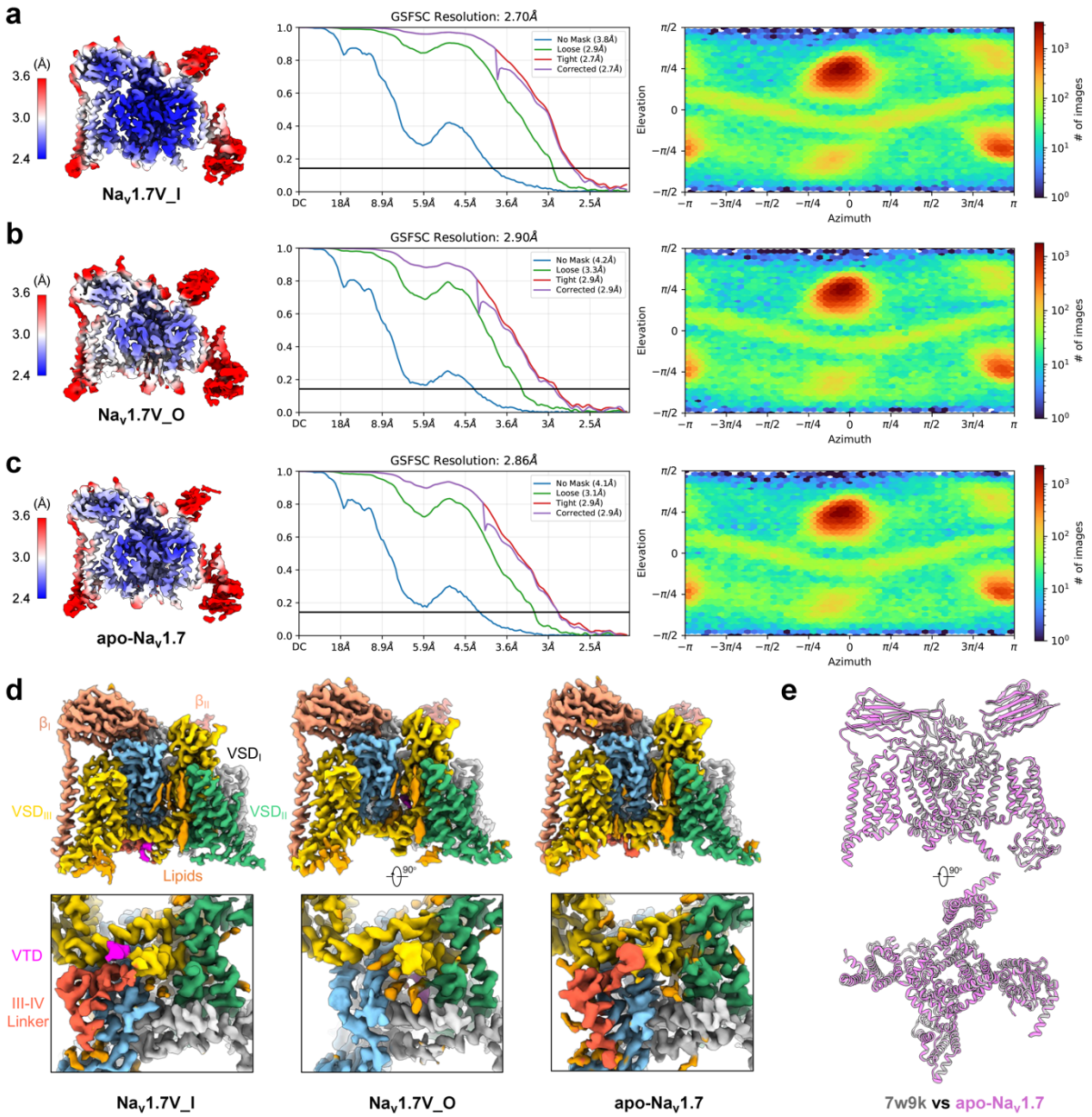

Supplementary Figure S3 | Cryo-EM analysis of the Na$_v$1.7-VTD complex reveals three distinct classes. (**a-c**) Local resolution estimations (*left*), gold-standard Fourier shell correlation (GSFSC) curves (*middle*), and angular distributions (*right*) for (**a**) classes Na$_v$1.7V_I, (**b**) Na$_v$1.7V_O, and (**c**) apo-Na$_v$1.7, respectively. (**d**) Overall cryo-EM 3D reconstructions (*top*) and corresponding zoomed-in views of the intracellular gate (*bottom*), highlighting the distinct ligand-binding features in each class. (**e**) Structural superposition revealed that the apo-Na$_v$1.7 class closely matches the previously reported apo structure (PDB: 7w9k), with an RMSD of 0.60 Å over 1,235 Cα atoms.

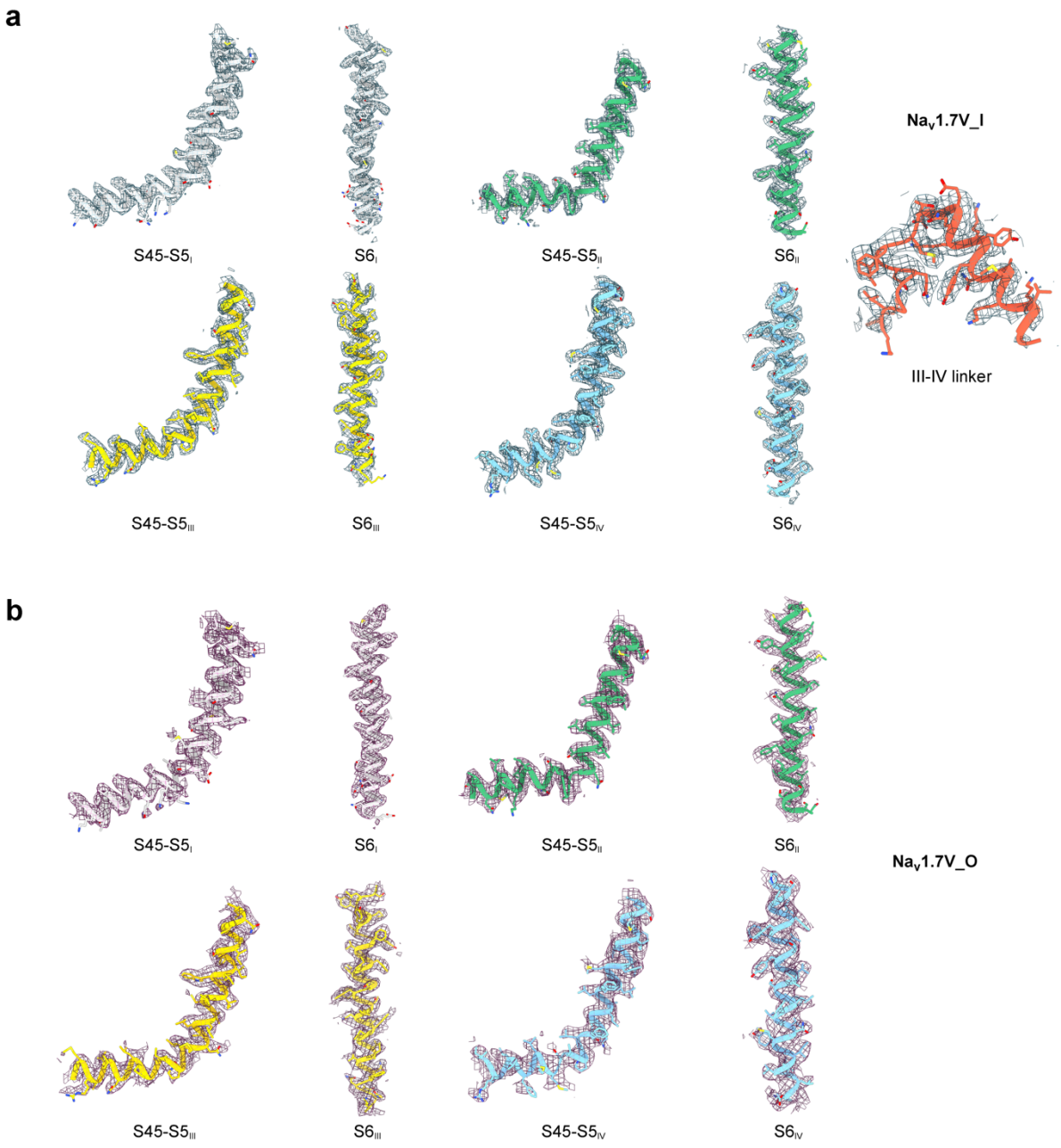

Supplementary Figure S4 | Local cryo-EM densities of the $Na_v1.7$-VTD pore domains. Local cryo-EM densities of the pore-domain helices are shown for (**a**) $Na_v1.7V_I$ class, and (**b**) $Na_v1.7V_O$ class, each exhibiting well-resolved features that corroborate the reconstructed maps and corresponding atomic models.

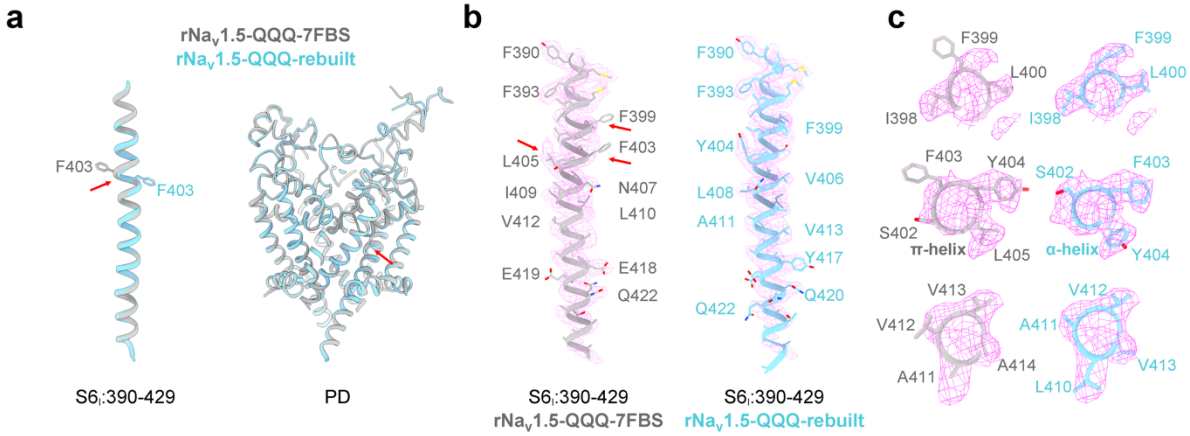

d

	rNaV1.5-QQQ-7FBS	rNaV1.5-QQQ-rebuilt
Protein residues	606	606
RMSD Bond lengths (Å)	0.010	0.003
RMSD Bond angles (°)	1.159	0.545
MolProbity score	2.66	1.23
Clashscore	16.74	4.56
Rotamer outliers (%)	3.75	0.79
CaBLAM outliers (%)	3.41	0.68
Ramachandran plot		
Favored (%)	91.61	98.15
Allowed (%)	8.22	1.85
Disallowed (%)	0.17	0.00

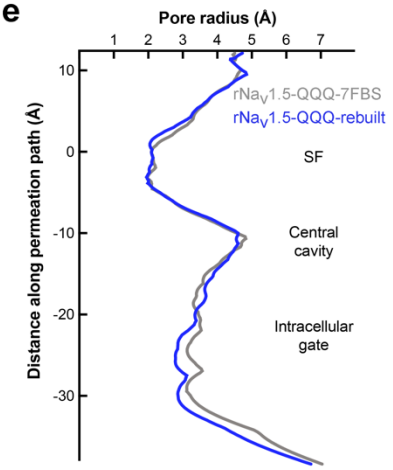

Supplementary Figure S5 | Validation and refinement of the rNa$_V$1.5-QQQ model. (**a**) Superposition of the original (PDB: 7FBS, grey) and rebuilt (cyan) pore-domain structures of rNa$_V$1.5-QQQ. The most significant change is the rebuilt α-helix spanning residues 400-403 within the S6$_I$ segment (*left*). Red arrows indicate the origin of the assignment error. (**b**) Model-to-density fit for the original and rebuilt rNa$_V$1.5-QQQ S6$_I$ segments within the deposited EM map (EMD-31519). Red arrows highlight examples of poorly fitted side chains in the original model that were corrected during refinement. (**c**) Close-up views of the S6$_I$ helix fit at each turn. The rebuilt model (cyan) shows improved density agreement, supporting an α-helical conformation at Phe403 instead of the previously assigned π-helix. (**d**) Quantitative metrics of model validation support the improved quality of the refined model. (**e**) Ion permeation path analysis indicates subtle alterations to the conduction path in the refined model compared to the original structure.

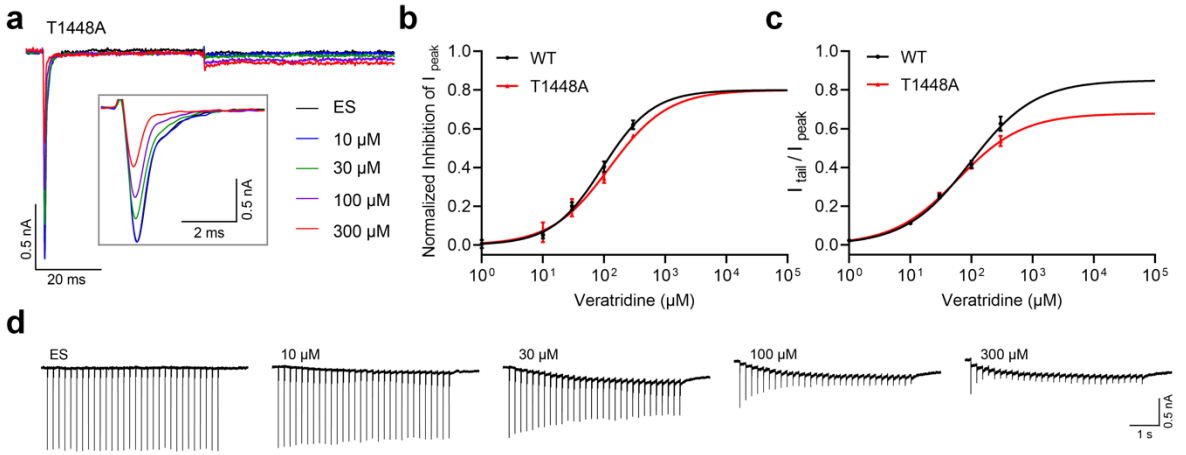

Supplementary Figure S6 | Functional characterization of veratridine modulation of hNa$_v$1.7-T1448A mutant. Single point mutation T1448A does not influence VTD-mediated Na$_v$1.7 modulation. (**a**) Representative traces for the measurement of VTD effects on Na$_v$1.7-T1448A currents. The protocol is the same as for the WT channel. Cells were held at -120 mV and depolarized to a test pulse to 0 mV for 50 ms. An enlarged view of the peak current is shown in the inset. (**b**) Concentration-response relationships for VTD-mediated peak current inhibition of Na$_v$1.7-T1448A compared to Na$_v$1.7-WT. (**c**) Concentration-response relationships for VTD-evoked accumulated tail current of Na$_v$1.7-T1448A compared to Na$_v$1.7-WT. (**d**) Representative traces illustrating the use-dependent modulation of VTD on Na$_v$1.7-T1448A, evoked by a 5-Hz train stimulation (30 pulses of 5-ms duration from –120 mV to 0 mV). The effect is also close to that on Na$_v$1.7-WT.

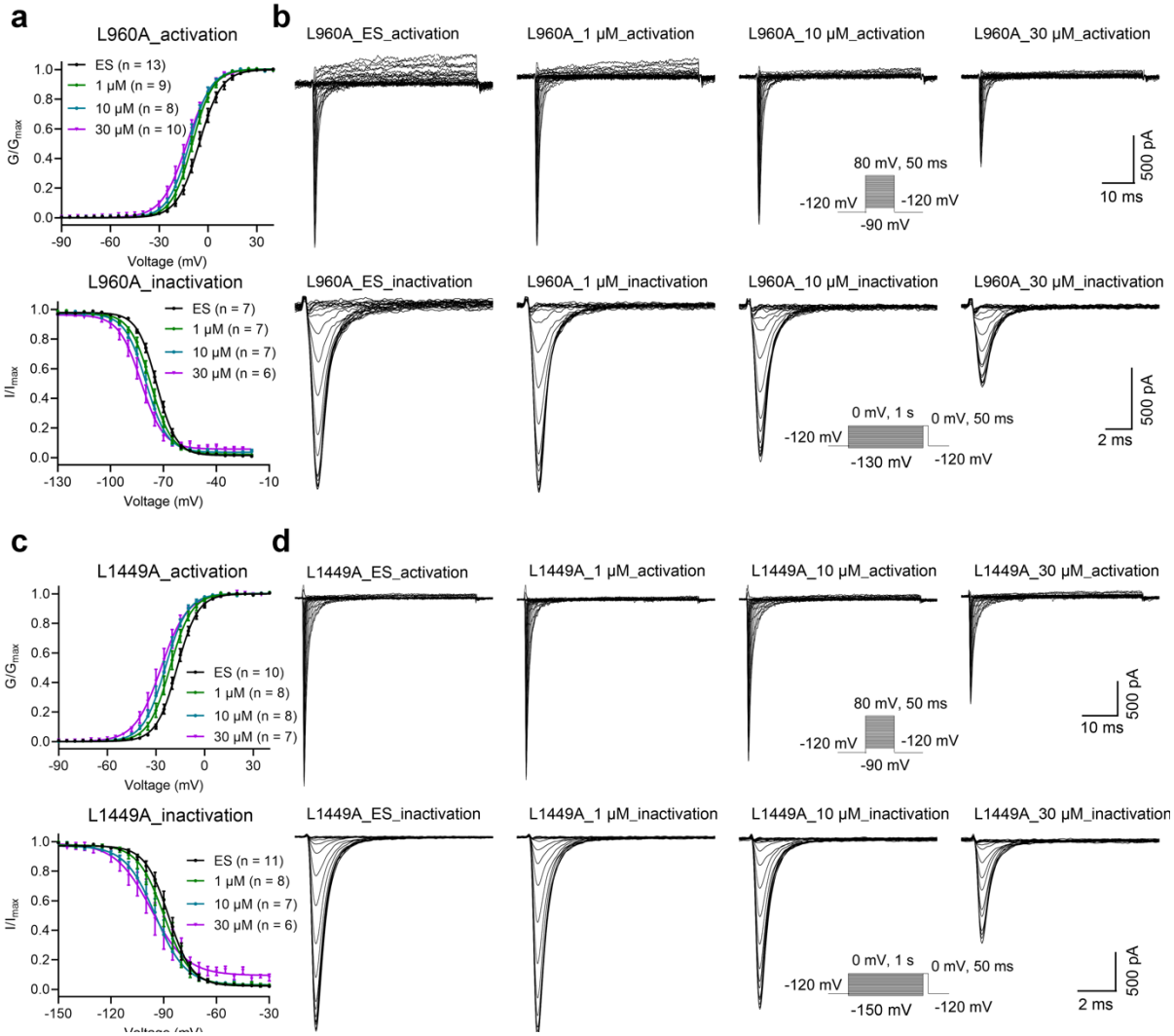

Supplementary Figure S7 | Functional characterization of veratridine modulation of hNa$_v$1.7-L960A and L1449A mutants. Voltage-dependent activation curves (*top*) and steady-state inactivation curves (*bottom*) of (**a**) Na$_v$1.7-L960A and (**c**) Na$_v$1.7-L1449A recorded under varying concentrations of veratridine. Representative current traces illustrating voltage-dependent activation (*top*) and steady-state inactivation (*bottom*) of (**b**) Na$_v$1.7-L960A and (**d**) Na$_v$1.7-L1449A in the presence of veratridine at the indicated concentrations. Inserts show the recording protocols.

Supplementary Table S1 | Parameters of the concentration-response relationships for veratridine-mediated inhibition of peak currents in hNa$_v$1.7 variants.

Parameters	**WT**		**L960A**		**T1448A**		**L1449A**	
IC_{50} (μM)	92.66 ± 18.41		27.56 ± 2.30 ****		122.6 ± 27.14		15.68 ± 0.97 ****	
P	/		<0.0001		0.6044		<0.0001	
k (mV)	1.06 ± 0.18		1.53 ± 0.20		0.91 ± 0.31		1.61 ± 0.17 *	
P	/		0.0708		0.5278		0.0335	
Top	0.80 ± 0.11		0.92 ± 0.04		0.80 ± 0.30		0.94 ± 0.02	
P	/		0.4049		0.9369		0.3253	
[VTD]	Mean ± SEM	n	Mean ± SEM	n	Mean ± SEM	n	Mean ± SEM	n
1 μM	0.005 ± 0.021	13	-0.016 ± 0.024	10	/	/	0.033 ± 0.025	9
10 μM	0.052 ± 0.017	17	0.158 ± 0.036	10	0.066 ± 0.051	2	0.302 ± 0.034	10
30 μM	0.201 ± 0.021	16	0.495 ± 0.030	11	0.193 ± 0.045	2	0.700 ± 0.022	10
100 μM	0.405 ± 0.028	15	0.799 ± 0.020	10	0.344 ± 0.024	2	0.886 ± 0.012	8
300 μM	0.620 ± 0.023	15	0.907 ± 0.007	7	0.565 ± 0.002	2	0.936 ± 0.005	8

*P < 0.05, ****P < 0.0001 versus Na$_v$1.7-WT. The extra sum-of-squares F test was used to compare the IC_{50}, slope factor (*k*) and top of concentration-response curves. Each data point represents mean ± s.e.m (standard deviation of mean), and n denotes the number of independently recorded cells.

Supplementary Table S2 | Parameters of the concentration-response relationships for veratridine-mediated enhancement of accumulated tail currents in hNa$_v$1.7 variants.

Parameters	**WT**		**L960A**		**T1448A**		**L1449A**	
EC_{50} (μM)	95.44 ± 16.62		/		53.87 ± 12.20		/	
P	/				0.6747			
k (mV)	0.82 ± 0.12				0.86 ± 0.14			
P	/				0.9175			
Top	0.85 ± 0.12				0.66 ± 0.07			
P	/				0.3194			
[VTD]	Mean ± SEM	n	Mean ± SEM	n	Mean ± SEM	n	Mean ± SEM	n
0 μM	0.013 ± 0.004	18	0.015 ± 0.002	13	0.017 ± 0.005	2	0.021 ± 0.005	10
1 μM	0.023 ± 0.004	10	0.021 ± 0.002	10	/	/	0.038 ± 0.010	9
10 μM	0.112 ± 0.006	12	0.067 ± 0.008	11	0.118 ± 0.007	2	0.055 ± 0.007	10
30 μM	0.252 ± 0.011	13	0.127 ± 0.006	11	0.256 ± 0.014	2	0.136 ± 0.018	6
100 μM	0.416 ± 0.019	13	/		0.406 ± 0.012	2	/	
300 μM	0.626 ± 0.037	11			0.536 ± 0.027	2		

The extra sum-of-squares F test was used to compare the IC_{50}, slope factor (*k*) and top of concentration-response curves. Each data point represents mean ± s.e.m (standard deviation of mean), and n denotes the number of independently recorded cells.

Supplementary Table S3 | Parameters of voltage-dependent activation of hNa$_v$1.7 variants with and without veratridine.

	Parameters	ES	1 μM	10 μM	30 μM	100 μM	300 μM
WT	$V_{1/2}$ (mV)	-17.21 ± 0.21	-21.77 ± 0.34 ****	-24.50 ± 0.21 ****	-26.45 ± 0.30 ****	-28.93 ± 0.37 ****	-31.68 ± 0.50 ****
	P	/	<0.0001	<0.0001	<0.0001	<0.0001	<0.0001
	k (mV)	7.00 ± 0.18	6.84 ± 0.29	6.17 ± 0.18 **	6.68 ± 0.26	7.03 ± 0.31	8.46 ± 0.43 ***
	P	/	0.5992	0.0013	0.2959	0.9420	0.0004
	n	16	10	13	12	12	12
L960A	$V_{1/2}$ (mV)	-5.449 ± 0.3097 ****	-9.642 ± 0.2729 ****	-11.40 ± 0.3363 ****	-12.94 ± 0.4201 ****	/	
	P	<0.0001	<0.0001	<0.0001	<0.0001		
	k (mV)	6.877 ± 0.2643	6.400 ± 0.2344	6.678 ± 0.2880	7.746 ± 0.3606 *		
	P	0.3531	0.1990	0.6259	0.0496		
	n	13	9	8	10		
L1449A	$V_{1/2}$ (mV)	-16.96 ± 0.24	-21.31 ± 0.36 ****	-24.22 ± 0.41 ****	-26.78 ± 0.55 ****	/	
	P	0.8391	<0.0001	<0.0001	<0.0001		
	k (mV)	6.43 ± 0.21 **	6.66 ± 0.31	6.86 ± 0.35	8.13 ± 0.47 ***		
	P	0.0090	0.5218	0.2658	0.0002		
	n	10	8	8	7		

**P < 0.01, ****P < 0.0001 versus Na$_v$1.7-WT on the condition of external solution (ES). **P < 0.01, ***P < 0.001, ****P < 0.0001 versus the corresponding variant of Na$_v$1.7 on the condition of external solution. The extra sum-of-squares F test was used to compare the $V_{1/2}$ and slope factor (*k*) of activation. Each data point represents mean ± s.e.m (standard deviation of mean) and n is the number of independently recorded cells.

Supplementary Table S4 | Parameters of voltage-dependent steady-state inactivation of hNa$_v$1.7 variants with and without veratridine.

	Parameters	ES	1 μM	10 μM	30 μM	100 μM	300 μM
WT	$V_{1/2}$ (mV)	-75.29 ± 0.23	-78.51 ± 0.40 ****	-79.28 ± 0.36 ****	-80.39 ± 0.36 ****	-83.69 ± 0.42 ****	-85.54 ± 0.53 ****
	P	/	<0.0001	<0.0001	<0.0001	<0.0001	<0.0001
	k (mV)	-6.06 ± 0.20	-6.41 ± 0.35	-6.54 ± 0.32	-6.42 ± 0.32	-6.83 ± 0.37 *	-6.63 ± 0.47
	P	/	0.3524	0.1792	0.3115	0.0488	0.2136
	n	19	11	14	14	13	9
L960A	$V_{1/2}$ (mV)	-73.91 ± 0.2360 ***	-77.26 ± 0.3081 ****	-79.83 ± 0.3592 ****	-82.73 ± 0.5390 ****	/	
	P	0.0004	<0.0001	<0.0001	<0.0001		
	k (mV)	-5.509 ± 0.2061	-5.977 ± 0.2700	-6.047 ± 0.3154	-6.372 ± 0.4740		
	P	0.1106	0.1700	0.1483	0.0683		
	n	7	7	7	6		
L1449A	$V_{1/2}$ (mV)	-87.29 ± 0.50 ****	-89.96 ± 0.81 **	-94.78 ± 0.97 ****	-97.19 ± 1.72 ****	/	
	P	<0.0001	0.0037	<0.0001	<0.0001		
	k (mV)	-6.73 ± 0.44	-7.45 ± 0.72	-8.59 ± 0.88 *	-10.14 ± 1.57 **		
	P	0.1216	0.3697	0.0405	0.0058		
	n	11	8	7	6		

***P < 0.001, ****P < 0.0001 versus Na$_v$1.7-WT on the condition of external solution (ES). *P < 0.05, **P < 0.01, ****P < 0.0001 versus the corresponding variant of Na$_v$1.7 on the condition of external solution. The extra sum-of-squares F test was used to compare the $V_{1/2}$ and slope factor (*k*) of inactivation. Each data point represents mean ± s.e.m (standard deviation of mean) and n is the number of independently recorded cells.

Supplementary Table S5 | Statistics for cryo-EM data and structural refinement.

	$Na_v1.7V_I$	$Na_v1.7V_O$
Data collection and processing		
Magnification	105,000	105,000
Voltage (kV)	300	300
Electron dose (e-/Å^2)	50	50
Defocus range (μm)	-1.2~-1.6	-1.2~-1.6
Pixel size (Å)	1.114	1.114
Symmetry	C1	C1
Total good particle	631,118	631,118
Final particles	335,177	133,758
Map resolution (Å)	2.7	2.9
FSC threshold	0.143	0.143
Refinement		
Map sharpening *B* factor (Å^2)	103.9	101.6
Model composition		
Non-hydrogen atoms	13,103	12,531
Protein residues	1,538	1,472
Ligands	26	25
B factors (Å^2)		
Protein	65.92	99.95
Ligand	110.59	116.04
R.m.s deviations		
Bond lengths (Å)	0.003	0.002
Bond angles (^{o})	0.527	0.499
Validation		
MolProbity score	1.39	1.37
Clashscore	7.15	6.80
Rotamer outliers (%)	0.22	0.08
CaBLAM outliers (%)	0.80	0.77
Ramachandran plot		
Favored (%)	98.69	98.69
Allowed (%)	1.31	1.31
Disallowed (%)	0.00	0.00

Supplementary Video S1 | **MD simulation trajectories.** The presented movie visualizes ion permeation events observed during 150-ns (one-tenth of the total simulation time) molecular dynamics simulation trajectories for the open-state structure $Na_v1.7V_O$ (*left*) and the rebuilt rNav1.5-QQQ model (*right*).

Supplementary Video S2 | **Proposed mechanism of fast inactivation in Na_v.** The movie presents a morph from the open-state structure ($Na_v1.7V_O$) to the inactivated state (PDB: 7W9M).